Electronic Supplementary Material (ESI)

The negatively charged $Cu_{1.33}S$ nanochains: endocytic pathway, photothermal therapy and toxic effect in vivo

Le Luo, Zhenghua Wang*

Key Laboratory of Functional Molecular Solids, Ministry of Education, College of Chemistry and Materials Science, Anhui Normal University, Wuhu 241000, People's Republic of China.

Table of Contents

1. Experimental Procedures

1.1 Chemicals

$CuSO_4 \cdot 5H_2O$ was purchased from Titan Scientific Co., Ltd. (Shanghai, China). Thioacetamide (TAA) was bought from Adamas Reagent Co., Ltd. Poly (sodium 4-styrenesulfonate) salt (M.W. 300,000) (PSS) was obtained from Alfa Aesar. Ascorbic acid (AA) was acquired from Aladdin. Fetal bovin serum (FBS) was purchased from Tianhang Biotech. Co., Ltd. (Zhejiang, China). Sucrose, phosphate buffered saline (PBS), and Roswell Park Memorial Institute 1640 medium (RPMI 1640) was purchased from Biosharp. Methyl-β-cyclodextrin (m-β-CD) was obtained from Macklin. Eosin, hematoxylin stain, and neutral balsam were bought from ZSGB-Bio. Deionized water was obtained from a Millipore Milli-Q system (Yamato, WG203). All of the chemicals were used as received without any further purification.

1.2 Instruments and Characterizations

Transmission electron microscopy (TEM) images were taken by a HT-7800 (Hitachi, Japan) microscope at an accelerating voltage of 100 kV. Vis−NIR absorption spectra were recorded with a U-4100 spectrophotometer (Hitachi, Japan). HAADF-STEM, and EDS elemental mapping images were performed on Talos F200S (Thermo Scientific). X-ray photoelectron spectroscopy (XPS) was operated by an ESCALAB 250Xi. The inductively coupled plasma mass spectrometry (ICP-MS) data were taken from Aglient 7800 (USA). Dynamic light scattering (DLS) was characterized by Zetasizer Nano ZSE. The photothermal images were taken by a SC300 infrared camera (Fluke TiR, USA). Bio-TEM images were conducted by FEI Tecnai Spirit.

1.3 Biosafety Assessment of $Cu_{1.33}S$ Nanochains

Sprague Dawley (SD) rats purchased from SPF Biotechnology Co. Ltd., Beijing, China. The rats were intravenously injected with either 300 μL nanochains saline solution containing 97.2 μg Cu or saline (control group) via the tail-vein. Blood was drawn (days 1, 3, 20) from abdominal arteries. The plasma supernatant was stored at -80 ℃ for biochemistry analysis by Xinrui automatic biochemical analyzer (XR220 Pluse). In addition, whole blood was collected, diluted, and analyzed using a

hematology analyzer (HLIFE, HF-3800). To investigate the tissue pathology, major organs as heart, liver, spleen, lung and kidney were harvested. They were fixed in 4% paraformaldehyde, embedded in paraffin, and sectioned into slices, which were stained by H&E staining for pathological analysis.

1.4 Blood Circulation Behavior of $Cu_{1.33}S$ Nanochains

For blood circulation analysis, healthy female SD rats (n= 3) were intravenously injected with 300 μL of nanochains solution containing 97 μg Cu via the tail-vein. Blood was drawn from the abdominal aorta at 0.5, 1, 2, 4, 6, 8, 24 and 72 h post injection. The concentration of nanochains was quantified with the concentration of copper determined by ICP-MS. The blood pharmacokinetic profile of nanochains was fitted with two-compartmental model using Origin 8.0 software.

1.5 Biodistribution of $Cu_{1.33}S$ Nanochains

To evaluate the distribution of the $Cu_{1.33}S$ nanochains in tumor and other tissues, 4T1 cells were injected subcutaneously into the flanks of female mice (24-26 g) to grow 4T1 murine breast tumors to (7.0±0.5 mm×5.1±0.1 mm). Then 200 μL nanochains solution containing 64.8 μg Cu were intravenously injected into four groups of mice bearing 4T1 tumor via the tail-vein. Then, the various tissues (i.e. tumor, heart, liver, spleen, lung, kidney) were harvested at 6, 10, 24, and 72 h post injection, and respectively treated with digesting solution overnight. The concentrations of Cu were measured by ICP-MS. The tumor slice were stained by uranyl acetate and alkaline lead citrate for 15 min respectively and then observed in bio-TEM (FEI Tecnai Spirit).

2. Supplementary Figures

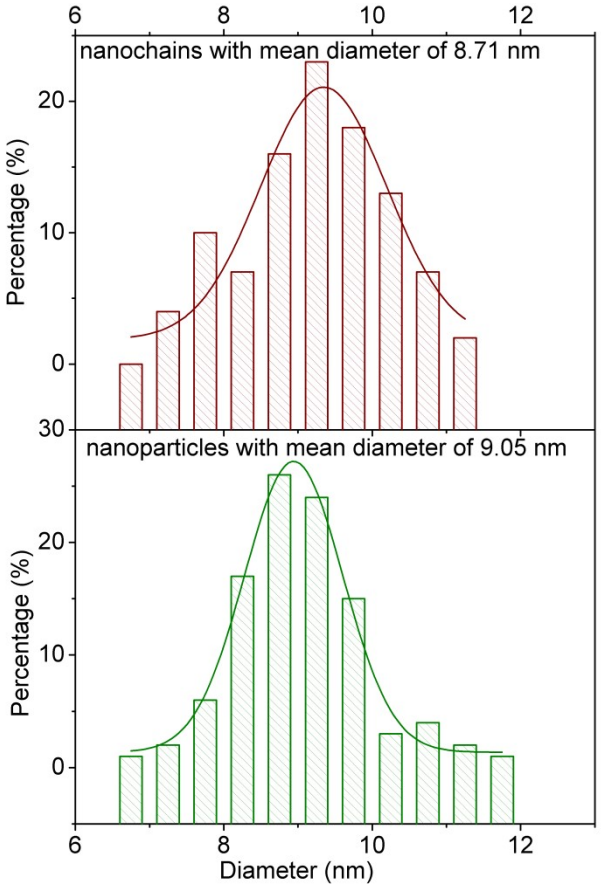

Fig. S1. Diameter distributions of the $Cu_{1.33}S$ nanochains and nanoparticles.

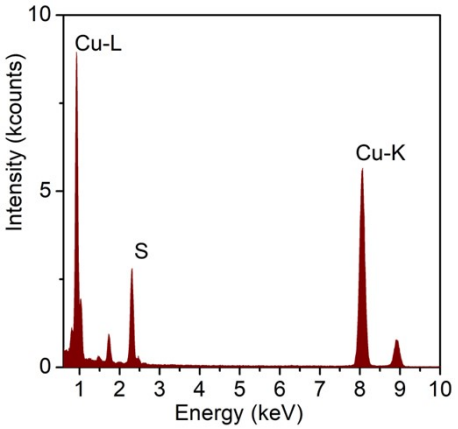

Fig. S2. Energy-dispersive X-ray spectroscopy analysis of the $Cu_{1.33}S$ nanochains.

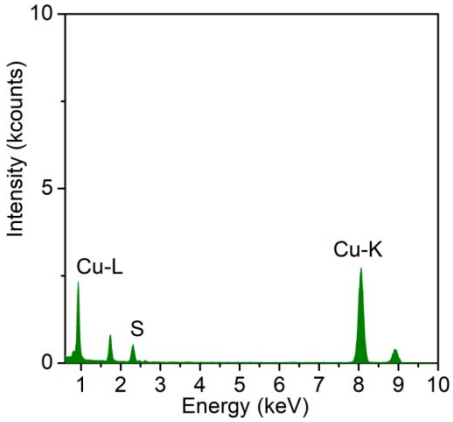

Fig. S3. Energy-dispersive X-ray spectroscopy analysis of the $Cu_{1.33}S$ nanoparticles.

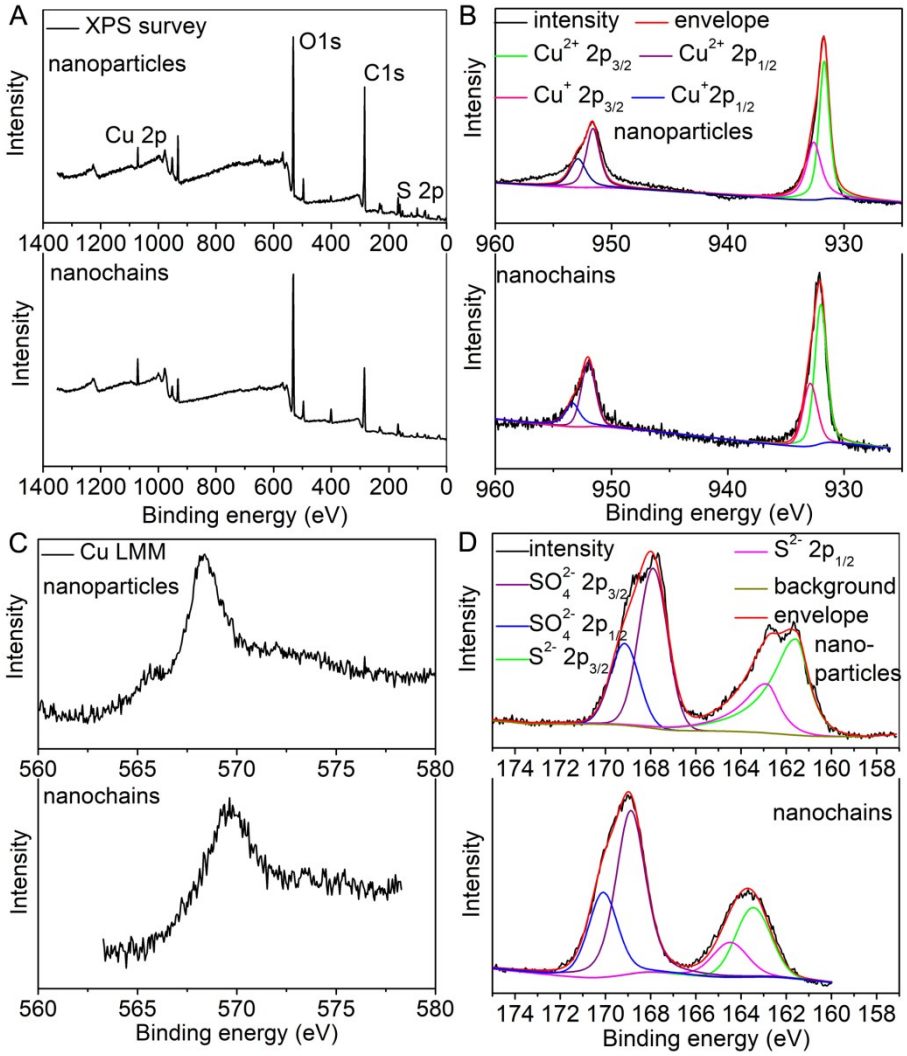

Fig. S4. (A) XPS survey spectra, (B) high-resolution XPS (HR-XPS) spectra of the copper 2p, HR-XPS spectra of the copper $2p_{1/2}$ and copper $2p_{3/2}$, (C) the AES spectrum in the Cu LMM region, and (D) the HR-XPS spectra of the sulfur $2p_{1/2}$ and $2p_{3/2}$ for $Cu_{1.33}S$ nanoparticles and nanochains.

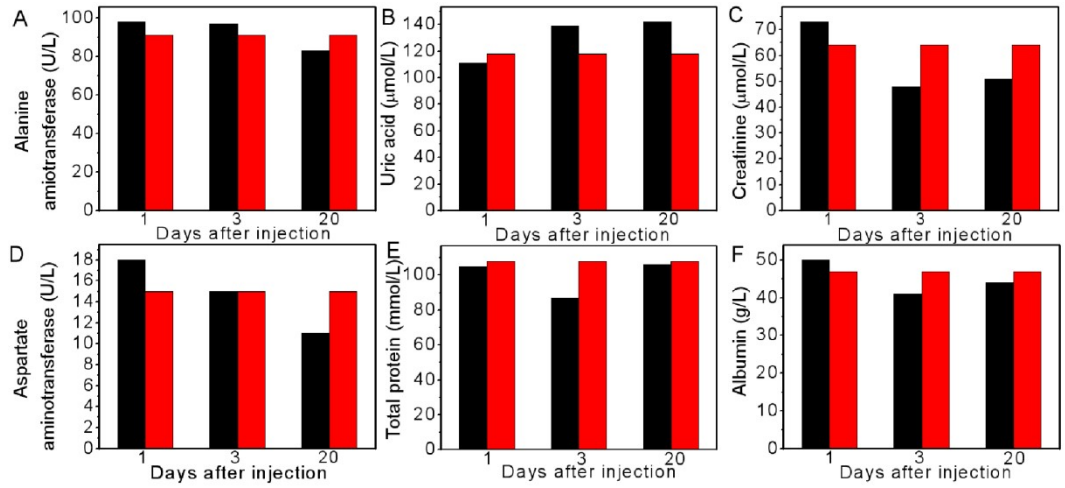

Fig. S5. Biochemical analysis on rats intravenously injected with nanochains (black bars) or saline (red bars) as controll: (A) Alanine amiotransferase, (B) Uric acid, (C) Creatinine, (D) Aspartate aminotransferase, (E) Total protein, (F) Albumin.

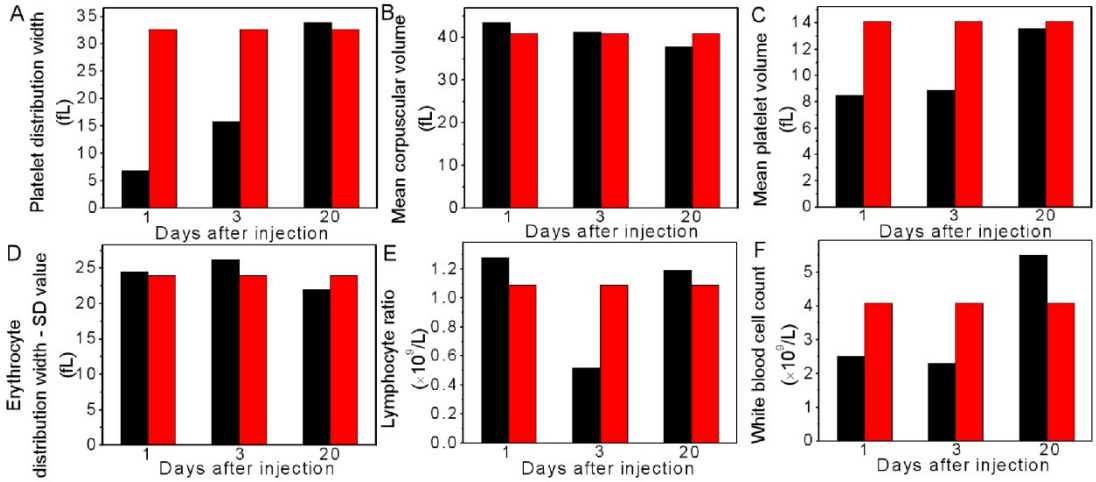

Fig. S6. Blood routine examination on rats intravenously injected with nanochains (red bars) or saline (black bars) as control: (A) Platelet distribution width, (B) Mean corpuscular volume, (C) Mean platelet volume, (D) Erythrocyte distribution width-SD value, (E) Lymphocyte ratio, (F) White blood cell count.

Fig. S7. Photographs of tissues and tumor harvested at different time points after nanochains injection.

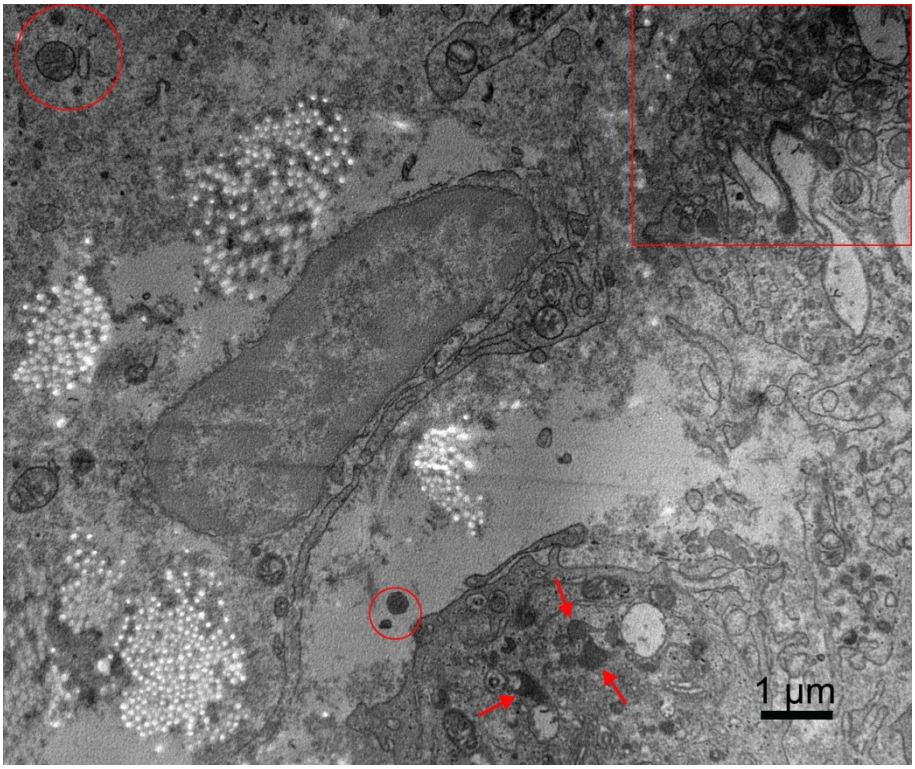

Fig. S8. Large scale bio-TEM image of tumor slice of the injected $Cu_{1.33}S$ nanochains mice post treat for 6 h.

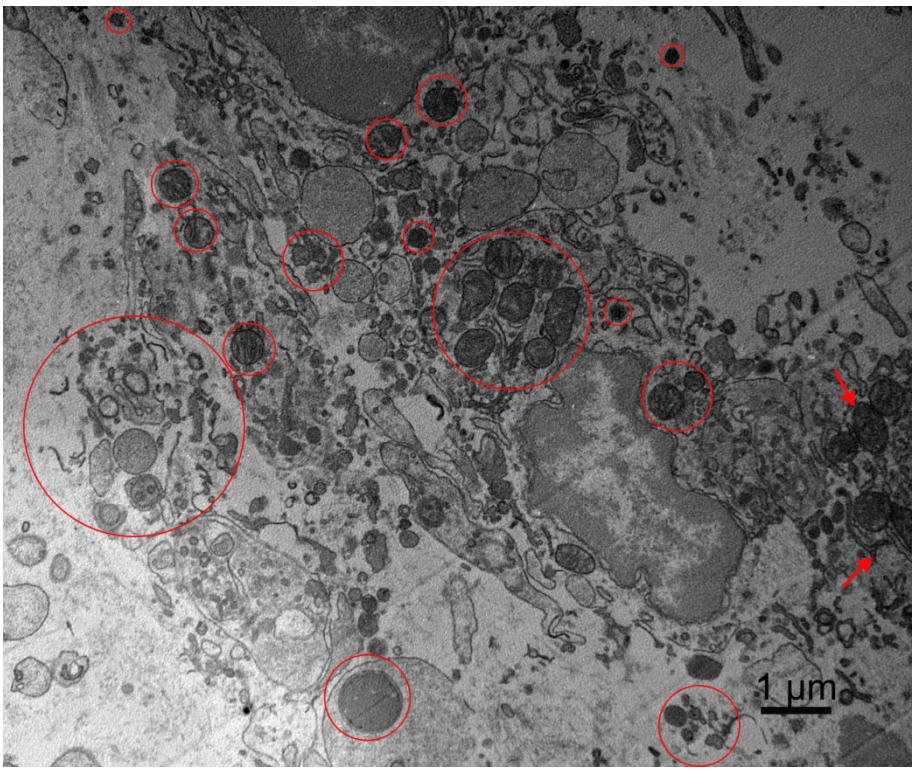

Fig. S9. Large scale bio-TEM image of tumor slice of the injected $Cu_{1.33}S$ nanochains mice post treat for 12 h.

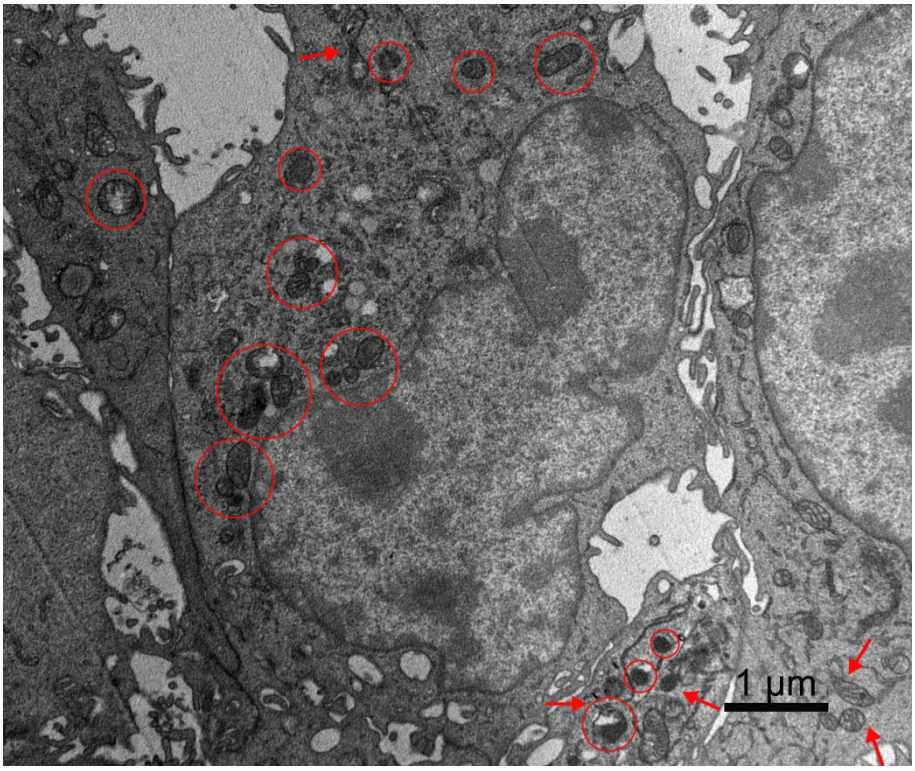

Fig. S10. Large scale bio-TEM image of tumor slice of the injected $Cu_{1.33}S$ nanochains mice post treat for 24 h.

3. Supplementary Tables

Table S1. Comparison of mass extinction coefficient and zeta potential of the as-symthesized nanochains and nanoparticle.

Samples	λ_{max}	$\alpha_{\lambda_{max}}$ (L g^{-1} cm^{-1})	Zeta potential (mV)
$Cu_{1.33}S$ nanochains	1220 nm	17.3	−46.8
$Cu_{1.33}S$ nanoparticles	1120 nm	60.8	−41.8

Table S2. Comparison of tumor accumulation value of the $Cu_{1.33}S$ nanochains with references.

References	Materials	Animal models	Max uptake (%ID/g)
S1	Au nanorods (Dimension: 2*10 nm)	Mice bearing U87MG tumor	7.8%
S2	CuS temperature sensitive nanoclusters	Mice bearing triple-negative breast tumor	8.02%
	CuS nanodots		3.27%
	CuS nanodots+Laser irradiation		3.70%
S3	Au nanorings (Thickness:50 nm)	Mice bearing subcutaneous U87MG tumors	~14%
	Au nanorings (Thickness: 25 nm)		13.6±1.6%
this work	$Cu_{1.33}S$ nanochains (Diameter: 8.7 nm)	Mice bearing 4T1 tumor	15%

Table S3. Comparison of photothermal therapy effect of the $Cu_{1.33}S$ nanochains with references.

Ref.	Material	Laser Power Density	Injection Dosage	ΔT (°C)	PTT Effects
S4	BODIPY nanoparticles	808 nm (0.32 W cm^{-2}, 5 min)	0.03 mg (intravenous injection)	20 (from 32 to 52)	inhibited the tumor growth for 15 days post-treatment
S5	borondifluoride bridged azafulvene complex	1064 nm (0.75 W cm^{-2}, 10 min)	300 μmol (intravenous injection)	18 (from 33 to 51)	eradicated without any recurrence for 15 days post-treatment
S6	Au multipod nanocrystals	1064 nm (1 W cm^{-2}, 10 min)	0.01 mg (intratumoral injection)	25 (from 25 to 50)	inhibited tumor growth for 16 days post-treatment
this work	$Cu_{1.33}S$ nanochains (diameter: 8.7 nm)	808 nm (1 W cm^{-2}, 10 min)	0.02 mg (intratumoral injection)	46 (from 33 to 79)	inhibited tumor growth for 13 days

References

S1. X. Tong, Z. Wang, X. Sun, J. Song, O. Jacobson, G. Niu, D. Kiesewetter, X. Chen, Size dependent kinetics of gold nanorods in EPR mediated tumor delivery, Theranostics, 2016, 6, 2039-2051.

S2. J. Ji, F. Ma, H. Zhang, F. Liu, J. He, W. Li, T. Xie, D. Zhong, T. Zhang, M. Tian, H. Zhang, H. Santos, M. Zhou, Light-activatable assembled nanoparticles to improve tumor penetration and eradicate metastasis in triple negative breast cancer, Advanced Functional Materials, 2018, 28, 1801738.

S3. Y. J. Liu, Z. T. Wang, Y. Liu, G. Z. Zhu, O. Jacobson, X. Fu, R. L. Bai, X. Y. Lin, N. Lu, X. Y. Yang, W. P. Fan, J. B. Song, Z. Wang, G. C. Yu, F. W. Zhang, H. Kalish, G. Niu, Z. H. Nie, X. Y. Chen, Suppressing nanoparticle-mononuclear phagocyte system interactions of two-dimensional gold nanorings for improved tumor accumulation and photothermal ablation of tumors, ACS Nano, 2017, 11, 10539-10548.

S4. W. B. Hu, X. F. Miao, H. J. Tao, A. Baev, C. Ren, Q. L. Fan, T. C. He, W. Huang, P. N. Prasad, Manipulating nonradiative decay channel by intermolecular charge transfer for exceptionally-improved photothermal conversion, *ACS Nano*, 2019, 13, 12006-12014.

S5. Z. P. Liu, Z. Y. Jiang, C. L. Zhang, X. Q. Wang, M. Yan, Z. X. Ling, Y. C. Chen, A borondifluoride-complex-based photothermal agent with an 80% photothermal conversion efficiency for photothermal therapy in the NIR-II window, *Angew. Chem. Int. Ed.*, 2021, 60, 2-11.

S6. J. J. Zhou, Y. Y. Jiang, S. Hou, P. K. Upputuri, D. Wu, J. C. Li, P. Wang, X. Zhen, M. Pramanik, K. Pu, H. W. Duan, Compact plasmonic blackbody for cancer theranosis in near-infrared II window, *ACS Nano*, 2018, 12, 2643-2651.